ELSEVIER

Journal of Materials Processing Technology 182 (2007) 369–373

Journal of Materials Processing Technology

www.elsevier.com/locate/jmatprotec

Characterization on electron beam welds and parameters for AZ31B-F extrusive plates

Chao-Ting Chi [a,b,*], Chuen-Guang Chao [a]

[a] *Department of Materials Science and Engineering, National Chiao-Tung University, Hsinchu 300, Taiwan, ROC*

[b] *System Manufacturing Center, Chung-Shan Institute of Science and Technology, P.O. Box 90008-14, Sanxia 237, Taipei, Taiwan, ROC*

Received 5 February 2006; received in revised form 11 August 2006; accepted 19 August 2006

Abstract

Recent years have seen a renewal of interest in magnesium alloys because of the extensive applications in the industry of 3C, aerospace and traffic. However, applications of magnesium alloys are still restricted by their poor formability. This can be improved by dividing the shape-complicated work piece into several easily-made parts and then combining into one. There are various kinds of defects in the weld under the interaction of AZ31B properties and welding conditions. These defects will produce obvious stress concentration and serious material damage. In this study, a home-made 11 mm-thick AZ31B extrusive plate was used. By operating and comparing the changeable parameters of electron beam welding (EBW), the condition was optimized as 100 mA, 50 kV, 60.6 mm/s and focus position at bottom. Seventy-eight percent and 91% of the base material strength were obtained by stress and non-stress concentration weldments, respectively. Meanwhile, the harmful influence of SC and grain coarsening reached at least 13% and 9%, respectively. With other worse parameters, the strength of AZ31B weldments were reduced by undercut, root concavity, cavities and heat-affected zone (HAZ).

Keywords: Electron beam welding; Optimum parameter; Stress concentration; Heat-affected zone

1. Introduction

Before the end of the Second World War, mass production of magnesium alloys were in demand for the fast developed aerospace and national defense industry. In 1942, the first manufactory to extract pure magnesium from sea water was built by American. It was a milestone for the application of magnesium alloys and the pursuance of lightweight metal. Thereafter, magnesium alloys were replaced by aluminum alloys and titanium alloys due to their low cost and strength, respectively. The major applications of magnesium alloys were then switched to civil purposes, such as vehicle and sporting goods. Currently, the use of magnesium alloys has been still increased in America and Europe in order to reduce the use of polymer materials.

Recent years have seen a renewal of interest in magnesium alloys because of the extensive applications in the industry of 3C, aerospace and traffic. This situation swells the demand of magnesium alloys, which are getting to be the important lightweight materials again. However, applications of magnesium alloys are restricted by their poor formability. Even though adopted die casting, their product reliability will be decreased due to the complicated gating system. Moreover, more expensive dies and fractional manufacture result in ballooning product price. If the shape-complicated work piece can be divided into several easily-made parts and then combined into one, this method will effectively improve these problems.

In the industry of aerospace and national defense, parts and assemblies are always joined cautiously. In particular, interface junctions are the major issues since many accidents result from them. Comparing with general mechanical fixing, welding usually provides better performance. Magnesium alloys can be jointed by usual welding methods [1,2], but their high reactivity requires a flux or vacuum environment for protection. In general, gas tungsten arc welding (GTAW or TIG welding) is the most prevalent among conventional welding methods. Nevertheless, the coarser grain, higher O content, and greater macropores (>0.1 μm [3]) can be induced in the weld [4] and degrade the mechanical properties of the weldment. Friction welding, a solid state welding method, can easily join in argon gas to prevent

* Corresponding author. Tel.: +88 691 6930 630.
E-mail addresses: joseph.mse92g@nctu.edu.tw (C.-T. Chi), c_g_chao@hotmail.com (C.-G. Chao).

0924-0136/$ – see front matter © 2006 Elsevier B.V. All rights reserved.
doi:10.1016/j.jmatprotec.2006.08.024

Table 1
Chemical compositions of AZ31B alloy is measured by ICP-AES and ICP-MS (wt%)

Element Material	Mg	Al	Zn	Mn	Si	Cu	Fe	P	Pb	Be
AZ31B	96.2467	2.8150	0.6395	0.2835	0.0094	0.0004	0.0025	0.0013	0.0008	0.0009

oxidation and combustion with 90% joint efficiency [5]. It is, however, difficult to get a precise measurement. Diffusion welding requires long heating time for bonding, while the coarsened grains and the oxidized joint interface decrease the weld strength [6]. Laser welding has much higher energy density and depth-to-width ratio [7,8] as compared with aforementioned methods. It can melt and solidify metal in a very short time to form finer grain, lower O content, and fewer micropores ($\leq$0.1 μm [3]) in the weld [4]. However, the energy limitations of laser welding restrict the fusion penetration depth in thicker work pieces [1], though with excellent focusing ability [7,8]. Based on these reasons, EBW will be the best choice among the welding technologies of magnesium alloys.

EBW was created in 1950's and used in nuclear industry. Because it could be achieved the highest precision in position and formed the highest depth-to-width ratio of weld, it could also be applied, undoubtedly, in the industry of aerospace and national defense [9]. In the early stage of EBW development, its equipments which required high vacuum level were not used extensively because of the high cost and low productivity. Subsequently, low and non-vacuum systems were developed to greatly reduce the working time, these equipments were finally accepted widely [10]. In 2001, Florian Banhart first successfully soldered 15 nm-diametral carbon nanotubes with EBW [11] and created the new era of welding history. This demonstration would be good for the research and development of ultra precision integrated circuit in the future.

For reasons mentioned above, EBW of magnesium alloys are very possible to become the most important technology for the welding of lightweight alloy. The authors choose this topic, not only because it is interesting, but also because it is an important current issue. So far, only few articles have been published on EBW of magnesium alloys [2,12–14]. The high cost of EBW equipments and magnesium alloys are the major causes. Therefore, it is worth examining the subject more closely.

In this study, the authors adjusted the variable parameters of EBW including beam current, accelerated voltage, welding speed, and focus position. Seventy-seven sets of specimens for home-made 11 mm-thick AZ31B extruded plate have been fabricated, and a comparison study has also been finished.

2. Experimental methods

In this study the research material used was a home-made AZ31B extrusive plate, which had a dimension of 105 mm × 60 mm × 12 mm. The outside of AZ31B-F plate about the welding area was removed 0.5 mm to avoid the influence of oxide layer. After two plates welded together by a butt joint process, their dimension became 105 mm × 119 mm × 11 mm. The variable parameters of EBW were arranged and combined in turn according to five fixed power values (3000, 3500, 4000, 4500 and 5000 W) under vacuum (3×10^{-5} torr) environment. At two parameters, there were three major repeated values and some minor unrepeated values in their specific regions – the former were beam current of 100, 125, 150 mA and accelerated voltage of 30, 40, 50 kV, while the latter were beam current of 60–167 mA and accelerating voltage of 20–50 kV. The conditions of welding speed (60.6, 73.3 and 86.0 mm/s) and the focus position (surface, middle and bottom of the plate) were the same among them. Only one parameter was changed at a time, so as to understand individual characteristic of these parameters.

The AZ31B-F weldments were cut into one metallographic and six tensile specimens along the extrusive direction. Their EBW paths which located at the center of gage length of the standard tensile specimens were perpendicular to longitudinal direction. Three of the specimens were milled finish on surface and bottom as non-stress concentration (NSC) specimens, while the other three remained the original weld appearance as stress concentration (SC) specimens. These specimens whose detailed dimensions according to ASTM B557-02 standard specification [15] were used for comparing the influence of stress concentration and measuring the strength of weld.

Since the phenomena of EBW of AZ31B-F were not easy to explain, this study would provide more evidence for them. The characteristic assessment of these weldments included chemical composition analysis of the material, tensile test of weldment, microstructure of weld cross section, X-ray diffraction (XRD) of crystalline, and distribution of micro-indentation hardness (Vickers, Hv) on the transverse plane. The parameters would be optimized in accordance with experimental results and examined later again.

3. Results and discussion

3.1. Chemical composition analysis

The chemical compositions of AZ31B-F plate analyzed using inductively coupled plasma-atom emission spectrometer and mass spectrometer (ICP-AES and ICP-MS): all content of chemical elements coincide with ASTM B275-02 standard specification (Table 1) [16].

3.2. Tensile test

In this study, the testing is the most convenient way from the viewpoint of measuring weldment strength so as to understand the influences of beam current, accelerated voltage, welding speed and focus position. Figs. 1 and 2 indicates that the ultimate tensile strength (UTS) of SC samples of AZ31B alloy clearly increases with increasing beam current and accelerated voltage, whereas it decreases with increasing welding speed. When the power is below 4000 W, this will cause incomplete joint penetration and result in occurrence of SC. But if the power is between 4000 and 5000 W, the strength of samples remained constant over nearly the entire period studied. While the fixed accelerated voltage or beam current is individually changed to another condition (30, 40 kV or 125, 150 mA), they will show the similar trend. However, there is no any apparent difference among the UTS of NSC samples. These curves remain horizontal when the condition changed. For reasons stated above, there should be no

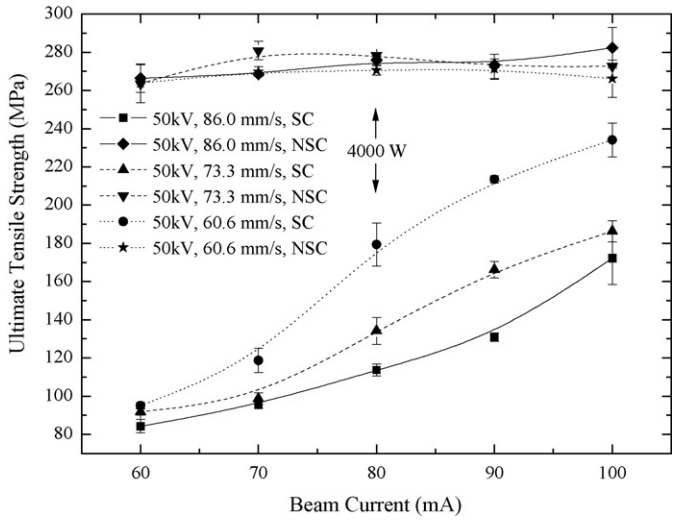

Fig. 1. Effect of beam current on the UTS of AZ31B weldments.

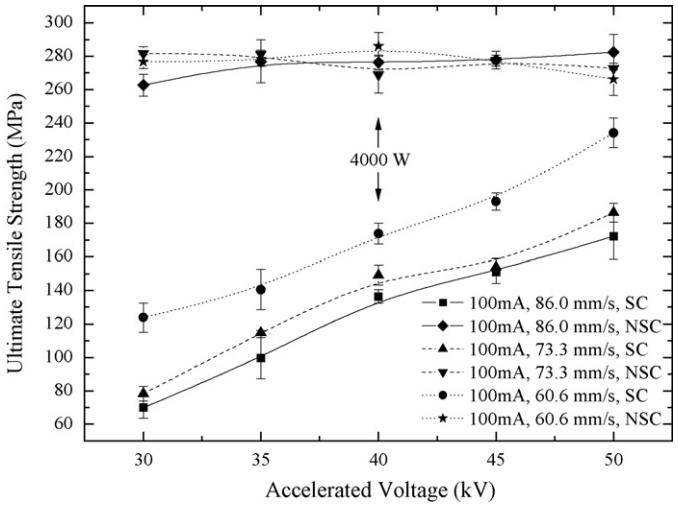

Fig. 2. Effect of accelerated voltage on the UTS of AZ31B weldments.

other special phase transformation in the weld when different energy was input by EBW.

Because of the lower boiling point (1090 °C) and melting point (650 °C) of pure magnesium and the higher energy density of EBW, AZ31B alloy in the weld will induce easily better fluidity during melting. Fig. 3 shows the appearance differences of weld channel at different focus positions. While the focus position of the electron beam is close to the surface of the work piece, the weld will produce worse spatter on the surface and lead to more apparent incomplete fusion penetration at the root. Since these areas will incur severe stress concentration, UTS values of the samples from top to bottom are, respectively, 153.9 MPa (Fig. 3(a)), 185.4 MPa (Fig. 3(b)) and 234.1 MPa (Fig. 3(c)) which exhibit an accurate reflection of the reality.

Judging from the above, the control parameters of the maximum UTS could be optimized with a beam current of 100 mA, accelerated voltage of 50 kV, welding speed of 60.6 mm/s, and focus position at bottom. The maximum value (234.1 MPa) of UTS for all SC samples would achieve 78% of UTS (296.9 MPa) for base material and the average value of UTS (270.5 MPa) for all NSC samples would reach 91% of UTS for base material. There was evidence showing that the impingement of SC reached at least 13%, the follow-up experimental results would have more to explain about the remaining 9% later on.

3.3. Microstructure observation

Fig. 4(a) shows the cross section of the worse weld. The UTS of the worst weldment only reached 151.3 MPa under the situation of complete fusion penetration. It is with a beam current of 100 mA, accelerated voltage of 45 kV, welding speed of 86.0 mm/s, and focus position at bottom. The undercut, root concavity and cavities become the fatal factors of weld fracture which will cause excessive SC and reduce the UTS value of weldments. The cross section and microstructure of the optimum weld are shown in Fig. 4(b)(c) and some precipitate particles are observed and concentrated in the fusion zone (FZ). According to the analysis of energy dispersive spectrometer (EDS) in Fig. 4(d), the chemical compositions of these precipitate particles with more Al and Zn contents than that of the base material are moved from the vicinities of these particles – their Al contents are 7.28, 0.55, 2.23 wt%, respectively, and their Zn contents are 5.78, 1.65, 1.82 wt%, respectively. These fractional scattering and small size of precipitate particles could only provide limited strengthen effect in the weld.

3.4. XRD analysis

The preferred orientation and special phase of these samples could be analyzed by XRD. As shown in Fig. 5, there is no the formation of other phases on the prewelding or postwelding samples and there is only few differences between the optimum and worse weldments. It is found that the high fraction of the (1 0 $\bar{1}$ 0) plane lies on the transverse plane of AZ31B extrusive plate before operating EBW. However, the preferred orientation will remain only in the (1 0 $\bar{1}$ 1) plane and the (0 0 0 2)

Fig. 3. Comparison of weld channel appearance at different focus positions of AZ31B-F plates (fixed condition: 100 mA, 50 kV, 60.6 mm/s) 2 mm. (a) Focus at surface (crest and root), (b) focus at middle (crest and root), (c) focus at bottom (crest and root).

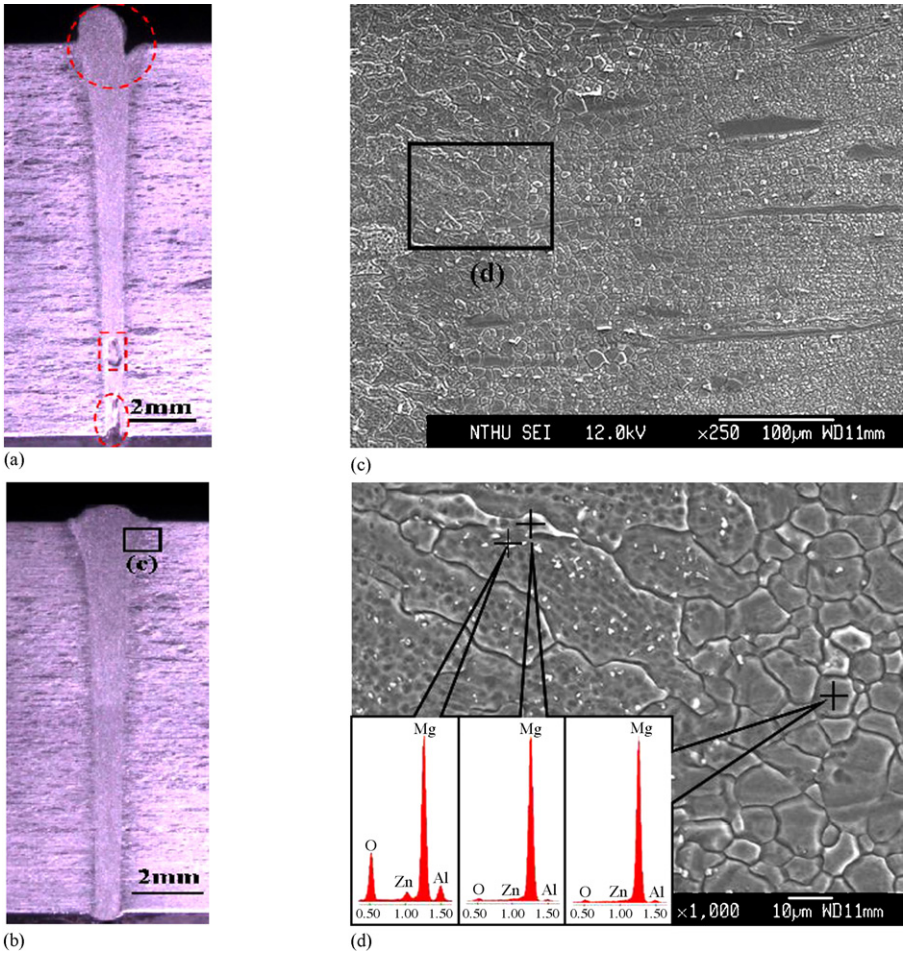

Fig. 4. Microstructure observation and EDS analysis for the cross section of worse and optimum weld. (a) Cross section of worse weld. (b) Cross section of optimum weld. (c) SEM photograph at the weld boundary. (d) SEM photograph at the weld boundary.

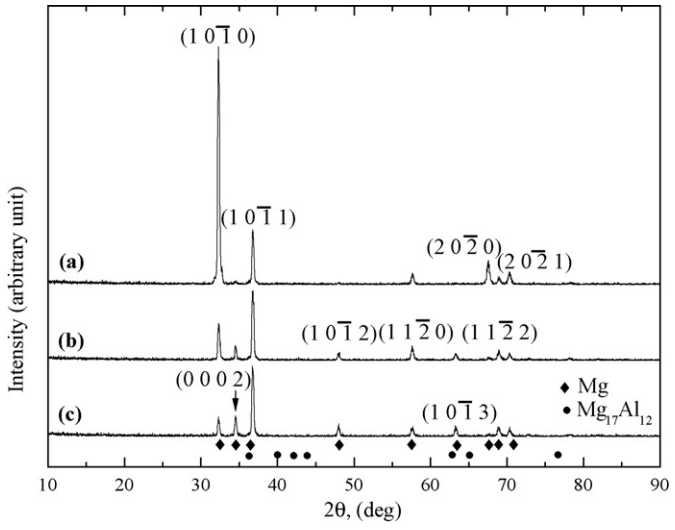

Fig. 5. Comparison of XRD spectrum for prewelding and postwelding sample of AZ31B-F. (a) Prewelding sample, (b) optimum weld sample, (c) worse weld sample.

orientation will increase with stepwise diffraction intensity after operating EBW. It follows from what has been said that the γ phase ($Mg_{17}Al_{12}$) is sole intermetallic compound, and the weldments will not form other phase transformation that affects its UTS. According to the experimental results of 77 sets of specimens, there was only one kind of fracture mode in practical tensile test – the crack randomly passed through the middle of the weld with initial and terminal position located in HAZ or the root concavity. What the phenomenon made clear at once was that the distribution of γ phase in the weld could only influence limitedly the strength of weldment.

3.5. Micro-indentation hardness test

The test positions of micro-indentation hardness test are indicated in Fig. 6(a) and the results are presented in Fig. 6(b). It can be seen that the curve of the optimum sample is more symmetrical than the worse one. The reason might be that the soften effect of coarse grain and the existence of cavities in the weld together caused the larger area of indentation and thus influenced the test value of the micro-indentation hardness. Therefore, there was a sudden dip in the random positions of the weld. From this viewpoint, the crack initiation and propagation of AZ31B weldments

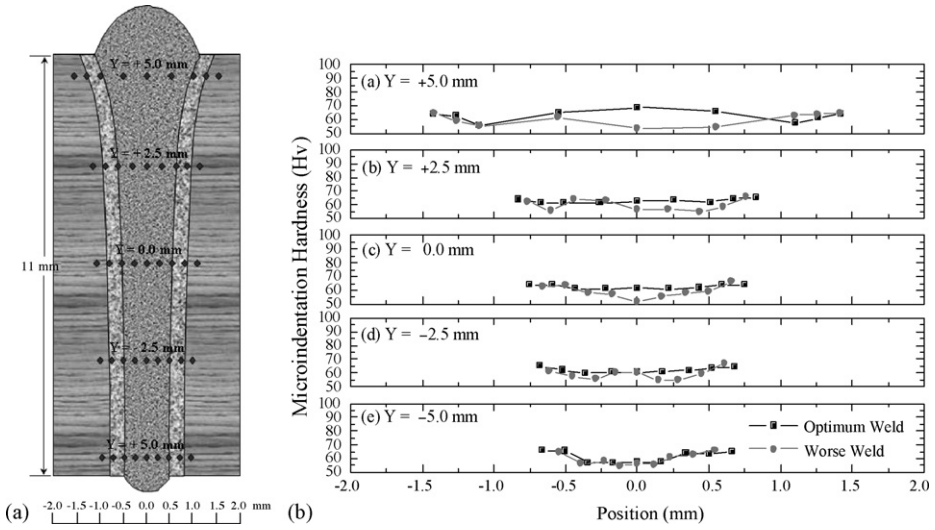

Fig. 6. Distribution relationship of micro-indentation hardness in the cross section of the weld. (a) Test position of micro-indentation hardness. (b) Micro-indentation hardness distribution of the optimum and worse sample.

would occur in the coarse grain area of HAZ (10 μm) and FZ (20 μm), or SC position. In other words, the coarse grain area of FZ and HAZ would be the major cause to reduce 9% of the UTS for NSC weldmemt at least.

4. Conclusions

In this study the parameters were optimized with a beam current of 100 mA, accelerated voltage of 50 kV, welding speed of 60.6 mm/s, and focus position at the bottom. The maximum value (234.1 MPa) of the UTS for the SC weldment of AZ31B-F and the average value (270.5 MPa) of the UTS for the NSC weldment of AZ31B-F lead to 78% and 91% of UTS for the base material, respectively. The harmful influence of SC and grain coarsening reached at least 13% and 9%, respectively.

The power was suitable between 4000 and 5000 W for welding 11 mm-thick AZ31B-F plates. Under other worse parameters, there were four factors reducing the UTS of EBW on AZ31B extrusive plates, which were undercut, root concavity, cavities and grain coarsening.

Acknowledgements

The authors heartily acknowledge the support from the National Science Council, ROC under Project No. NSC 93-2623-7-182-002. The authors also thank C.L. Chang and Z.G. Chang of System Manufacturing Center of Chung-Shan Institute of Science and Technology for technical assistance.

References

[1] M.M. Avedesian, H. Baker, Magnesium and Magnesium Alloys, ASM International, USA, 1999.
[2] X. Cao, M. Jahazi, J.P. Immarigeon, W. Wallace, A review of laser welding techniques for magnesium alloys, J. Mater. Process. Technol. 171 (2006) 188–204.
[3] H. Haferkamp, U. Dilthey, G. Träger, I. Bbumeste, M. Niemeyer, Beam welding of magnesium alloys, Magnes. Alloys Appl. (1998) 595–600.
[4] Z. Sun, J. Wei, D. Pan, Y.K. Tan, Comparative evaluation of tungsten inert gas and laser welding of AZ31 magnesium alloy, Sci. Technol. Weld. Join. 7 (2002) 343–351.
[5] K. Ogawa, H. Yamaguchi, H. Ochi, T. Sawai, Y. Suga, Y. Oki, Friction welding of AZ31 magnesium alloy, Weld. Int. 17 (2003) 879–885.
[6] H. Somekawa, H. Watanabe, T. Mukai, K. Higashi, Low temperature diffusion bonding in a superplastic AZ31 magnesium alloy, Scr. Mater. 48 (2003) 1249–1254.
[7] A. Weisheit, R. Galun, B.L. Mordike, CO_2 laser beam welding of magnesium-based alloys, Weld. J. (1998) 149s–154s.
[8] T. Asahina, Pulsed YAG laser weldability of magnesium alloys, Weld. Int. 19 (2005) 23–28.
[9] G. Thomas, V. Ramachandra, R. Ganeshan, R. Vasudevan, Effect of pre- and post-weld heat treatments on the mechanical properties of electron beam welded Ti-6Al-4V alloy, J. Mater. Sci. 28 (1993) 4892–4899.
[10] Z. Sun, R. Karppi, The application of electron beam welding for the joining of dissimilar metals: an overview, J. Mater. Process. Technol. 59 (1996) 257–267.
[11] F. Banhart, The formation of a connection between carbon nanotubes in an electron beam, NanoLetters 1 (2001) 329–332.
[12] S.F. Su, J.C. Huang, H.K. Lin, N.J. Ho, Electron beam welding behavior in Mg-Al based alloys, Metall. Mater. Trans. 33A (2002) 1461–1473.
[13] C. Vogelei, D. Dobeneck, I. Decker, H. Wohlfahrt, Strategies to reduce porosity in electron beam welds of magnesium die-casting alloys, Magnes. Alloys Appl. (2000) 191–199.
[14] U. Draugelates, B. Bouaifi, J. Bartzsch, B. Ouaissa, Properties of non vacuum electron beam welds of magnesium alloys, Magnes. Alloys Appl. (1998) 601–606.
[15] ASTM B557-02. Standard Test Method of Tension Testing Wrought and Cast Aluminum and Magnesium Alloy Products, 2002, pp. 1–15.
[16] ASTM B275-02. Standard Practice for Codification of Certain Nonferrous Metals and Alloys, Cast and Wrought, 2002, pp. 1–5.